THERMALLY ACTIVATED DISLOCATION CREEP MODEL FOR PRIMARY WATER STRESS CORROSION CRACKING OF NiCrFe ALLOYS

M. M. Hall, Jr.
Bettis Laboratory
Westinghouse Electric Corporation
West Mifflin, Pennsylvania 15122

ABSTRACT

There is a growing awareness that environmentally assisted creep plays an important role in intergranular stress corrosion cracking (IGSCC) of NiCrFe alloys in the primary coolant water environment of a pressurized water reactor (PWR). The expected creep mechanism is the thermally activated glide of dislocations. This mode of deformation is favored by the relatively low temperature of PWR operation combined with the large residual stresses that are most often identified as responsible for the SCC failure of plant components. Stress corrosion crack growth rate (CGR) equations that properly reflect the influence of this mechanism of crack tip deformation are required for accurate component life predictions.

A phenomenological IGSCC-CGR model, which is based on an *apriori* assumption that the IGSCC-CGR is controlled by a low temperature dislocation creep mechanism, is developed in this report. Obstacles to dislocation creep include solute atoms such as carbon, which increase the lattice friction force, and forest dislocations, which can be introduced by cold prestrain. Dislocation creep also may be environmentally assisted due to hydrogen absorption at the crack tip. The IGSCC-CGR model developed here is based on an assumption that crack growth occurs by repeated fracture events occurring within an advancing crack-tip creep-fracture zone. Thermal activation parameters for stress corrosion cracking are obtained by fitting the CGR model to IGSCC-CGR data obtained on NiCrFe alloys, Alloy X-750 and Alloy 600. These IGSCC-CGR activation parameters are compared to activation parameters obtained from creep and stress relaxation tests. Recently reported CGR data, which exhibit an activation energy that depends on yield stress and the applied stress intensity factor, are used to benchmark the model. Finally, the effects of matrix carbon concentration, grain boundary carbides and absorbed hydrogen concentration are discussed within context of the model.

Keywords: stress corrosion cracking, crack growth rate, models, creep, NiCrFe alloys

INTRODUCTION

Recently discovered intergranular stress corrosion cracking (IGSCC) of Alloy 600 components in the primary water circuits of commercial nuclear power reactors[1] has renewed interest in obtaining a more fundamental understanding of the IGSCC of NiCrFe alloys. An improved understanding of IGSCC and the availability of a physically based quantitative IGSCC crack growth rate (CGR) model could potentially prevent significant economic losses for electric-power utilities that operate nuclear reactors. Unfortunately, a thorough scientific understanding of stress corrosion mechanisms does not exist today and cannot reasonably be expected for some time.

However, reliable models having engineering utility often can be developed for complex physical processes using phenomenological modelling methods. A phenomenological model of environmentally assisted crack growth must be functionally descriptive of the physical processes that are considered to be controlling the crack growth rate. Mechanistic models and the results of controlled laboratory experiments provide insight into the selection of the appropriate mathematical relationships. In developing the phenomenological model, all model variables and parameters are chosen so as to be relatable to engineering parameters. The model parameters are obtained by fitting the model to the available experimental data. The range of each parameter may have to be statistically broadened to obtain satisfactory comparisons between predictions of the model and field experience. To gain acceptance for use, the model must describe all features of the data considered important and no assumption or prediction of the model can be in contradiction with other known experimental facts and established physical understanding. When successfully applied, this phenomenological approach results in engineering methods of component failure prevention that are logical, internally

consistent and are less reliant on engineering judgement.

Evidence for the Influence of Dislocation Creep in SCC

There is a growing awareness that environmentally assisted creep plays an important role in primary water stress corrosion cracking of NiCrFe alloys. Was and co-workers[2-4] have reported on the influence of microstructure on the IGSCC and creep deformation of controlled impurity Alloy 600-type alloys in high purity water. Their results show that creep modes of fracture play an important role in IGSCC of these alloys. They conclude that dislocation-controlled creep is the operative creep mechanism based on their observation of large stress exponents in their creep rate-stress correlations. Bousier et al.[5] have reported on the influence of mechanical parameters and the water environment on the IGSCC and creep deformation of Alloy 600 and the creep deformation of Alloy 690 in pressurized water reactor (PWR) primary water. Based on their constant extension rate and stress controlled creep tests, they conclude that strain rate is the mechanical parameter that controls the IGSCC crack propagation rate. Their creep test results show that the high-stress low-temperature creep rates of Alloy 600 and Alloy 690 in water are two to three times the rates attained in air.

Thermally Activated Dislocation Creep Model

Due to the relatively low temperature of PWR operation and the large residual stresses that are most often identified as responsible for IGSCC failures of reactor components,[6] the expected creep mechanism is thermally activated glide of dislocations. This deformation mechanism is enabled by the thermal agitation of the metal lattice and can operate at temperatures less than about 0.35 of the melting temperature. The lattice friction stress and short range obstacles combine to establish a threshold stress for dislocation slip. As the temperature is reduced, the thermal energy available to overcome obstacles to dislocation glide is reduced and the yield stress increases. This is illustrated by the temperature dependence of the Alloy 600 yield stress as shown by the data of Mulford and Kocks[7] in Fig. 1. Indicated in this figure is the so-called athermal temperature, T_o, at which thermal activation is sufficient to overcome short range obstacles but not long range obstacles. Analysis of these data yields an athermal temperature of 668 K. The yield stress at this temperature is due to long range obstacles. It is termed the athermal stress and is designated here as the threshold stress, σ_{th}.

As shown by Kocks, et al.[8] in their treatise on the thermodynamics and kinetics of dislocation slip, the rate equation that relates creep strain rate, $\dot{\varepsilon}$, to temperature, T, and the applied stress, σ, can be written as:

$$\dot{\varepsilon} = \dot{\varepsilon}_s \exp\left(-\frac{\Delta G(\sigma)}{RT}\right). \qquad (1)$$

In this equation ΔG is the Gibbs free energy and R is the universal gas constant. The pre-exponential factor, $\dot{\varepsilon}_s$, is an intrinsic strain rate that is proportional to the density of mobile dislocations, the distance between short range obstacles and the thermal-activation frequency.

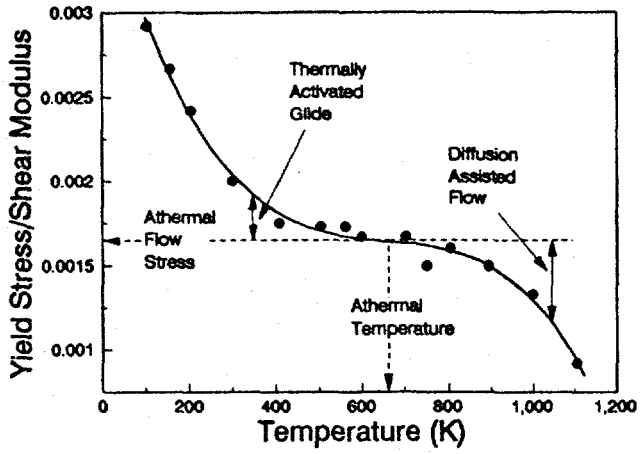

FIGURE 1. Alloy 600 Yield Stress Normalized by the Shear Modulus. Data From Ref. 7.

As shown in the Appendix, Eq.(1) can be specialized to represent creep by the thermally activated glide of dislocations. The applied stress component that is required to overcome resistance to deformation by this mechanism is commonly called the "effective" stress. A normalized effective applied stress as defined in the Appendix, is given by

$$\frac{\sigma^*}{\sigma_s^*} \equiv \frac{\sigma - \sigma_{th}}{\sigma_s - \sigma_{th}}. \qquad (2)$$

The subscript s refers to the maximum or "saturation" internal stress generated in overcoming the obstacles to dislocation glide at absolute zero. For stresses above the saturation stress, dislocations can find no equilibrium positions. Consequently, large scale slip, followed by a rapid approach to mechanical instability, will occur.

As shown in the Appendix, the deformation rate equation can be expressed in terms of the effective stress and energy parameters:

$$\dot{\varepsilon} = \dot{\varepsilon}_s \exp\left\{-\frac{\Delta H_o^*}{RT^*}\left[1 - \left(\frac{\sigma^*}{\sigma_s^*}\right)^p\right]^q\right\}. \qquad (3)$$

The asterisk indicates effective parameters as defined in the Appendix. The stress exponent p in Eq.(3) has a value less than or equal to one and greater than or equal to zero. A value of 1 is chosen for q. The effective activation enthalpy, ΔH_o^*, is the activation energy associated with the short-range obstacles only. The effective temperature, T^*, is defined by

$$\frac{1}{T^*} \equiv \frac{1}{T} - \frac{1}{T_o}. \qquad (4)$$

IGSCC - CGR MODEL DEVELOPMENT

We assume that stress corrosion crack advance occurs by a process of creep fracture of a crack tip region having a characteristic size, r_c. Repetition of this process results in sustained crack growth. If a critical creep strain, ε_c, is required for fracture of this zone, the crack growth rate is

$$\dot{a} = \frac{r_c \dot{\varepsilon}_{ct}}{\varepsilon_c}. \qquad (5)$$

The size, r_c, of this crack-tip creep-fracture zone (CFZ), depends on the micromechanism of crack advance[9], which may be influenced by environmental effects and dimensions of microstructural features, within and surrounding the CFZ.

The Alloy 600 creep data of Boursier, et al.[5] show that the creep strain rate decreases with time, which is consistent with the expectation that strain hardening will dominate any recovery mechanism that may operate at the low temperatures assumed for a thermally activated creep mechanism of IGSCC. Therefore the crack tip strain rate, $\dot{\varepsilon}_{ct}$, in the above equation is taken to represent the average rate during the time between CFZ fracture events.

Crack Tip Stress

We assume that during the time interval between CFZ fracture events the crack is stationary and that the creep deformation is confined within the CFZ. Furthermore, the CFZ is assumed to be small, compared to the dimensions of the crack tip plastic zone, so that the variation of stress within the CFZ is small. The stress within the crack tip CFZ will decrease somewhat due to creep relaxation during the interval between fracture events. However, we assume that the CFZ stress is constant in time and is established by the time-independent stress that exists at the boundary of the CFZ and the plastic zone into which the IGSCC crack advances when the CFZ fractures.

We now introduce material parameters K_{th} and K_s. These parameters are defined so that the applied stress within the CFZ is equal to the threshold stress, σ_{th}, and the saturation stress, σ_s, when the applied stress intensity factor has the values K_{th} and K_s, respectively. Note that the saturation stress intensity factor, analogous to σ_s, is a mechanical instability parameter that has a maximum value at absolute zero. With the introduction of the threshold and saturation stress intensity factors, a normalized effective applied stress intensity factor can be defined, analogous to Eq.(2), by

$$\frac{K^*}{K_s^*} \equiv \frac{K - K_{th}}{K_s - K_{th}}. \qquad (6)$$

We now establish a phenomenological relationship between the normalized effective applied stress within the CFZ and the normalized effective applied stress intensity factor, which are defined by Eq.(2) and Eq.(6), respectively. An analytical relationship that relates the stress within the crack tip plastic zone to the applied stress intensity factor has been derived by Hutchinson,[10] Rice and Rosengren[11]. This relationship is derived from the deformation theory of plasticity for conditions of small scale plasticity and is given by

$$\sigma = \sigma_o \left(\frac{K}{\sigma_o \sqrt{\alpha r}} \right)^{\frac{2}{n+1}}. \qquad (7)$$

In this equation σ_o is the material flow stress, K is the applied stress intensity factor, r is the distance from the crack tip, n is the inverse of the strain hardening exponent and α is a slowly varying function of n having a value of 4π for plane strain and for stresses within the elastic limit (n = 1).

Eq.(7) shows that, within the plastic zone, which surrounds the CFZ, there is a nonlinear relationship between the local stress and the stress intensisty factor. We *assume* that, within the CFZ, a mathematically similar relationship exists between the effective stress and the effective stress intensity factor. Using this assumption, for $r \le r_c$, we can write:

$$\sigma^* = bK^{*m}. \qquad (8)$$

In this equation, b is a constant and m is expected to be a function of the strain hardening exponent, 1/n.

Using the normalizations introduced above in Eq.(2) and Eq.(6), Eq.(8) can be written

$$\frac{\sigma - \sigma_{th}}{\sigma_s - \sigma_{th}} = \left(\frac{K - K_{th}}{K_s - K_{th}} \right)^m. \qquad (9)$$

Eq.(9) can now be substituted into Eq.(3) to obtain the crack

tip strain rate, which can in turn be substituted into Eq.(5) to obtain an expression for the IGSCC crack growth rate.

IGSCC Crack Growth Rate Equation and Apparent Activation Energy

Now the crack growth rate equation, Eq.(5), becomes

$$\dot{a} = \frac{r_c \dot{\varepsilon}_s}{\varepsilon_c} \exp\left\{-\frac{\Delta H_o^*}{RT^*}\left[1-\left(\frac{K-K_{th}}{K_s-K_{th}}\right)^p\right]\right\}. \quad (10)$$

The apparent activation energy, Q, is given by

$$Q = \Delta H_o^*\left[1-\left(\frac{K-K_{th}}{K_s-K_{th}}\right)^p\right]. \quad (11)$$

Note that, in order to avoid unnecessarily introducing another stress exponent, the stress intensity factor exponent, p, in these equations, should be understood as the product of the stress exponent, p, and stress intensity factor exponent, m, in Eq.(3) and Eq.(8), respectively.

These equations were fit to IGSCC data obtained on Alloy 600 materials that, due to application of a range of cold prestrain, have a range of yield stress, and therefor, a range of strain hardening. Fitting Eq.(10) to these IGSCC data confirmed that, for values of n less than about 4, the stress intensity factor exponent p is equal to 2/(n+1), as suggested by Eq.(7). However, an alternate expression for p, which has 2/(n+1) as a limit for small values of n, is required to obtain a good fit for materials having large n (large yield strength). This is believed to be due to extraplolation beyond the data range for which the expression for n, Eq.(15), was derived.

Fitting Eq.(11) to the IGSCC data showed that, when the normalized effective stress intensity approaches 1, the apparent activation energy does not reduce to zero as predicted. To account for this, Eq.(11) was modified:

$$Q = \Delta\tilde{H} + \Delta H_o^*\left[1-\left(\frac{K-K_{th}}{K_s-K_{th}}\right)^p\right]. \quad (12)$$

A similar modification of Eq. (10) is provided below as Eq.(13). The physical meaning of this added activation enthalpy term is discussed below.

IGSCC CRACK GROWTH RATE DATA AND DATA CORRELATIONS

There are few primary water IGSCC crack growth rate data, obtained on NiCrFe alloys, that are suitable for benchmarking the IGSCC-CGR model. The best available data are from the work by Shen and Shewmon[12] and Speidel and Magdowski[13]. However, there are limitations to each of these data sets. Both sets of data were obtained on displacement controlled specimens, which results in a decreasing stress intensity factor as crack growth occurs. Crack growth rates were determined by Shen and Shewmon using in-situ measurements of crack length but their tests were conducted in steam, instead of water. Speidel and Magdowski obtained crack growth rates from measurements of average crack extension divided by the total exposure time. Their rates do not, therefore, account for the time to the onset of IGSCC crack growth. The Shen-Shewmon data obtained on Alloy X-750 and Alloy 600 are shown in Fig. 2 and Fig. 4. The Speidel-Magdowski data obtained on Alloy 600 are shown in Fig. 3, Fig. 5 and Fig. 6. Note that the best fit Arrehnius curves for each data set in Fig. 2 and Fig. 3 were adjusted slightly to intersect at a common athermal temperature, T_o. The Shen-Shewmon data are best fit using an athermal temperature of 682 K while the Speidel-Magdowski data could be fitted reasonably well using the value of 668 K obtained from the data in Fig. 1. Results of the data fitting are given in Table I in the Discussion section. The expression for the inverse hardening exponent, n in Eq.(15), was obtained from the stress-strain data reported by Webb and Hall[14]. In this equation, S_y is the yield stress.

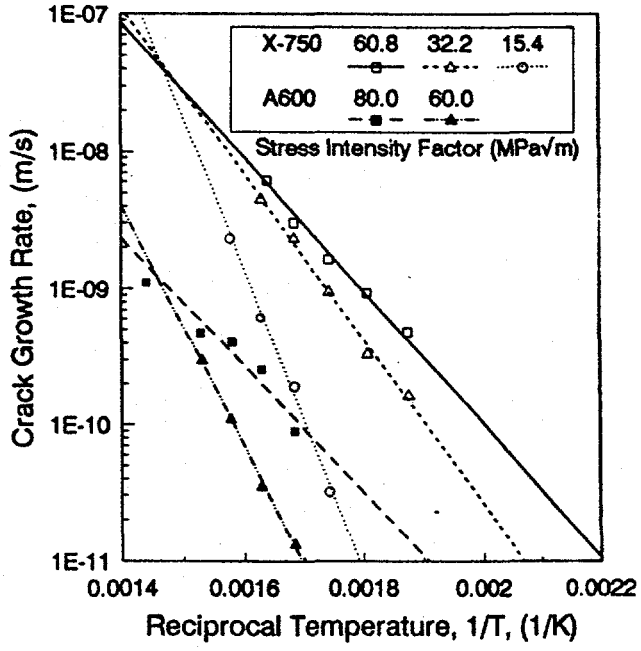

FIGURE 2. Effect of Temperature and Stress Intensity Factor on Crack Growth Rate. Data From Ref. 12.

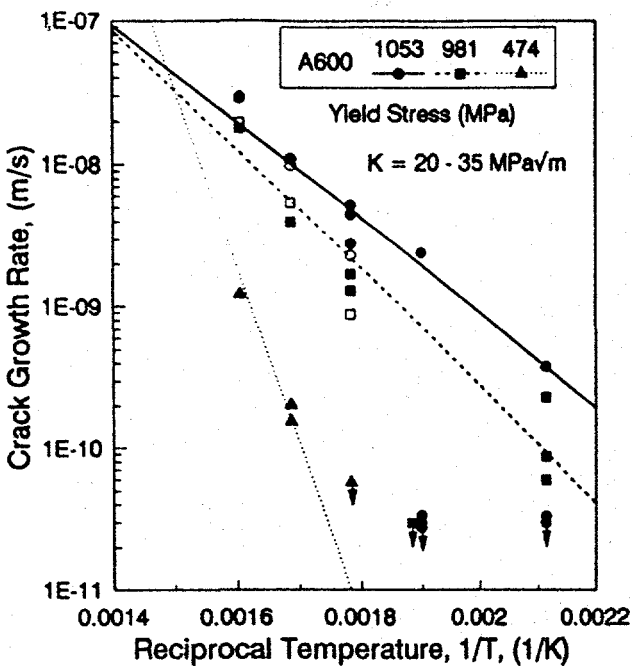

FIGURE 3. Effect of Temperature and Yield Stress on Crack Growth Rate. Solid symbols represent data from Ref. 13. Open symbols were obtained from data correlations for K = 30 MPa√m.

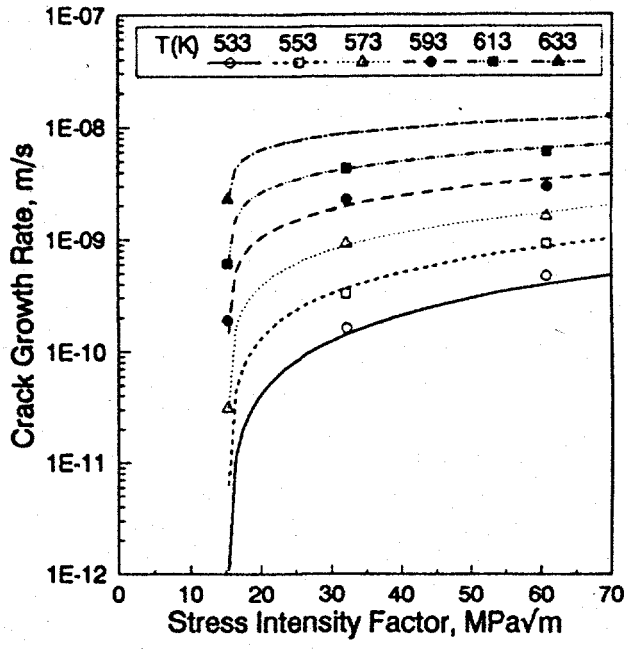

FIGURE 4. Alloy X-750 Crack Growth Rate as Function of the Stress Intensity Factor. Data From Ref. 12.

DISCUSSION

The data in Fig. 2 through Fig. 6 have several interesting features that are correctly predicted by our IGSCC-CGR model. First, consistent with the model predictions, the negative slopes of each of the Arrehnius curves (which are proportional to the apparent activation energies, Q) in Fig. 2 and Fig. 3 decrease with both increasing applied stress intensity factor and increasing yield stress. Second, these data can be fitted well with curves that intersect, as the model requires, at the athermal temperature, T_o. Third, there is an apparent threshold stress intensity factor evident in Fig. 4 and Fig. 5. Finally, the slopes of the log-crack growth rate versus log-stress intensity factor curves in Fig. 6 decrease with increasing temperature and yield stress and increase slightly with increasing stress intensity factor consistent with the model predictions. The magnitude of these slopes are equivalent to the stress exponent in a more conventional "power law" SCC rate equation.

The activation enthalpies, ΔH_o^*, for X-750 and A600 in Table I are nearly equal, being about 388 kJ/mole (4.1 eV). Sirois and Birnbaum[15] found activation enthalpies of 1.9 eV and 2.9 eV in stress relaxation and differential temperature tests of pure Ni and Ni-C, respectively. The larger value found for the more complex engineering alloys modelled here is not surprising given the potential for a greater variety of microstructural barriers to thermally activated slip. Moreover, the carbon content of the simple Ni-C alloy used in Sirois and Birnbaum's study was 0.025 weight percent (w/o) as compared to 0.04 w/o to 0.10 w/o, respectively in the Shen-

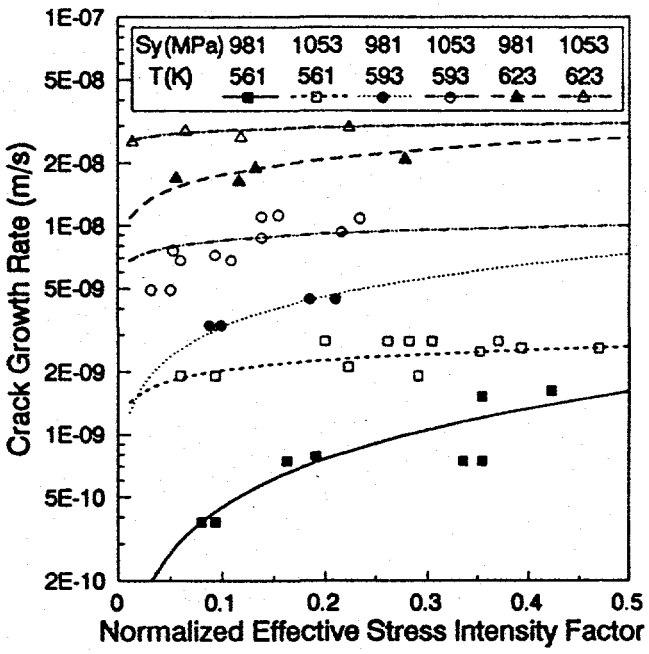

FIGURE 5. Alloy 600 Crack Growth Rate as Function of the Normalized Effective Stress Intensity Factor. Data From Ref. 13.

Shewmon and Speidel-Magdowski A600 materials. Bandy and van Rooyen[16] found that the apparent activation energy for initiation of primary water IGSCC in Alloy 600 tubing increased as the carbon concentration increased. Their data show an increase in Q of about 126 kJ/mol (1.3 eV) as carbon increases from 0.02 w/o to 0.06 w/o. Therefore, the value of 4.1 eV found here for the activation enthalpy compares favorably to the values of Sirois and Birnbaum considering

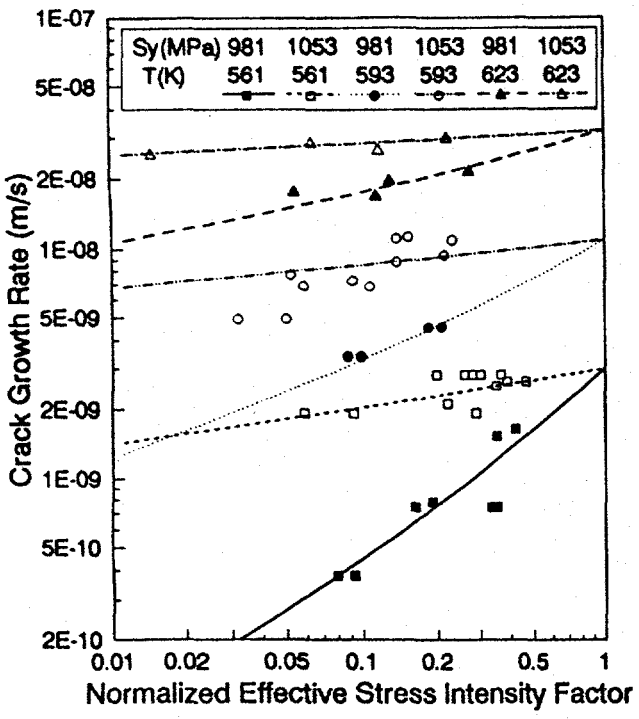

FIGURE 6. Alloy 600 Crack Growth Rate as Function of the Normalized Effective Stress Intensity Factor. Data From Ref. 13.

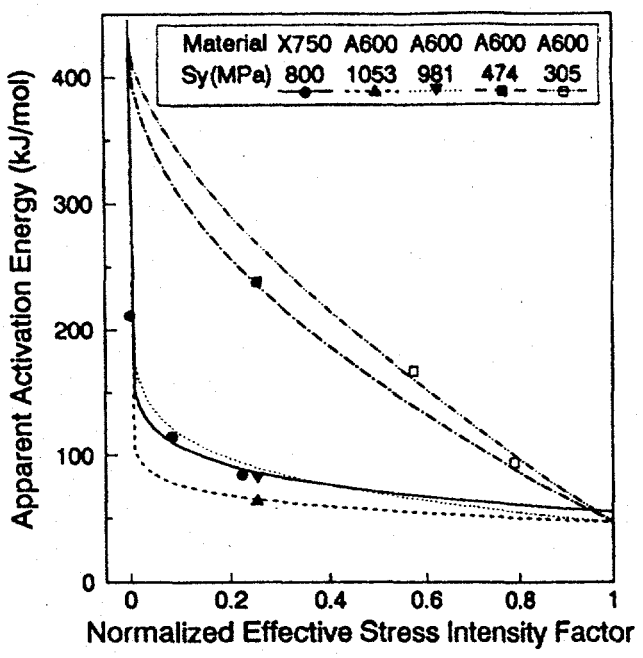

FIGURE 7. Apparent Activation Energy as Function of the Normalized Effective Stress Intensity Factor Showing the Effect of Yield Stress. Curves are derived from Ref. 13 data; open symbols represent A600 Q values from Ref. 12 data.

the higher carbon content of the alloys that were used to obtain the data used in this study.

Figure 7 shows the effect of stress intensity factor and yield stress on the apparent activation energy, Q, as predicted by Eq.(12). The Q values derived from Figure 2 and Figure 3 are shown for comparison. Note that Q values obtained from the Shen-Shewmon A600 data are in good agreement with the predictions based on the Eq.(12) correlation of the Speidel-Magdowski data. Note also that the Q correlations for Alloy X-750 and A600 are very similar for similar yield stresses.

Figure 7 also shows that, as the normalized effective stress intensity factor approaches 1, the apparent activation energy approaches a value of about 52 kJ/mol for both Alloy X750 and Alloy 600. If thermally activated glide were the only process contributing to the crack growth rate, then the apparent activation energy should approach 0. Since it does not, there appears to be an additional thermally activated rate process acting in series with thermally activated glide. The apparent activation energy for this process is approximately equal to the activation enthalpy reported by Rota et al.[17] (50 kJ/mol) for hydrogen diffusion in Alloy 600. We conclude that the model as currently formulated (Eq.(13)) is consistent with a hydrogen assisted creep mechanism of crack growth.

The model predicts that an increase in the activation enthalpy leads to a reduction in the creep rate, which results in a reduced crack growth rate. This prediction is supported by the results of Was et al.[3] who showed that an increase in solute carbon concentration from 0.002 w/o to 0.032 w/o results in about 3 orders of magnitude decrease in the creep rate of controlled purity Alloy 600-type alloys. They furthermore showed that, in a controlled extension rate IGSCC test of these alloys, higher solute carbon concentration results in a significant reduction in the relative amount of IGSCC.

In addition to demonstrating that solute carbon increases the activation enthalpy for dislocation creep, Sirois and Birnbaum showed that hydrogen, in their Ni-H and Ni-C-H alloys, causes a reduction in the activation enthalpy. Their results show that an addition of about 11 weight parts per million (wppm) hydrogen to the Ni-C-H alloy results in a reduction in the activation enthalpy by 0.9 eV (87 kJ/mole). At this rate, an increase of 4 wppm, which is the hydrogen solubility in unstressed Alloy 600 at 633 K, would increase the creep rate by about a factor of three at low stress and assuming an initial activation enthalpy of about 388 kJ/mole. This prediction compares favorably to the creep test results reported by Boursier et al.[5] who report a factor of two increase in creep rate for Alloy 600 and Alloy 690 when tested in water. They also report increased crack growth rates due to an increase of the hydrogen overpressure in their controlled extension rate tests.

Note that the IGSCC-CGR model developed here does not predict the observation by Boursier et al. that susceptibility to IGSCC first increases then decreases with increased hydrogen overpressure. This effect may be related to corrosion film stability, which is not a feature explicitly considered in the model development.

A final observation is that there is more than an order of magnitude difference between the pre-exponential terms in

	$$\dot{a} = \dot{a}_o \exp\left\{-\frac{\Delta\tilde{H}}{RT^*} - \frac{\Delta H_o^*}{RT^*}\left[1 - \left(\frac{K-K_{th}}{K_s-K_{th}}\right)^p\right]\right\} \quad (13)$$

Data Source	Shen-Shewmon Ref. 12		Speidel-Magdowski Ref. 13
Temperature Range	593 K - 693 K		473 K - 623 K
Material	X750	A600	A600
$\dot{a}_o$ (m/s)	4.3E-8	1.2E-9	4.0E-8
ΔH^*_o (kJ/mol)	390.1	Not Analyzed	385.1
$\Delta\tilde{H}$ (kJ/mol)	55.2	Not Analyzed	47.1
T_o (K)	682	682	668
K_{th} (MPa$\sqrt{m}$)	15.35	Not Analyzed	6.37
K_s (MPa$\sqrt{m}$)	219.8	Not Analyzed	99.9
p	0.0623	$p = 1+0.4281\ln(1/n)$ (14)	
n	≈ 6	$1/n = 0.256\ln(1559.3/S_y)$ (15)	

Table I. Crack Growth Rate Equation Parameters. There are insufficient Alloy 600 data from Ref. 12 to obtain most parameters.

the A600 CGR equations. This difference is not understood. It is speculated that the difference is brought about by differences in heat treatment. The heat treatment histories of these materials and their resulting microstructures are not detailed by the authors. Both materials are reported as received in the hot formed condition. However, the as-received strength and carbon concentration of the Speidel-Magdowski material are high, as compared to that of the Shen-Shewmon material; 474 MPa versus 305 MPa, and 0.10 w/o versus 0.06 w/o, respectively.

The CGR equation preexponential has two factors that, within the context of the model, influence the crack growth rate but are not developed here. These are the critical strain, ε_c, and the characteristic distance, r_c, in Eq.(5). Both are expected to be influenced by the heat treatment and the carbon concentration.

The critical creep strain for advancing the crack is expected to be a function of the local crack tip hydrogen concentration. This in turn is expected to be dependent upon the balance between the rates of hydrogen production and absorption at the crack tip with the rate of hydrogen diffusion away from the creep fracture zone. Grain boundary carbides may act simply to retard hydrogen production and absorption by limiting exposure of a less corrosion resistant matrix to the water. The rate of hydrogen loss is controlled by the hydrogen diffusion rate, which may be influenced by microstructural and strain induced trapping of hydrogen within the creep fracture zone, potentially at grain boundary carbide-matrix interfaces. Finally, since they are a dominant grain boundary feature, grain boundary carbides may influence the characteristic distance over which the creep fracture process operates.

CONCLUSIONS AND SIGNIFICANCE

A primary water stress corrosion crack growth rate model has been developed for NiCrFe alloys X-750 and Alloy 600 based on an assumption that the IGSCC growth rate is controlled by the kinetics and thermodynamics of a thermally activated low temperature creep mechanism.

Phenomenological features of the best available stress corrosion crack growth rate data are well correlated using this model. The model correctly predicts an effect of both stress intensity factor and yield stress on the apparent activation energy and an effect of both yield stress and temperature on the stress intensity factor dependence of the crack growth rate.

The thermal-activation enthalpies obtained by analysis of IGSCC crack growth rate data are consistent with independent measures of these parameters. The potential effects of the corrosive environment, matrix carbon and grain boundary carbides on the IGSCC crack growth rate can be rationalized within context of the model. This is an area for additional research.

Crack growth rate equations of the type developed here have application to engineering concerns for reactor power plant component performance. Application of the model allows interpolation and extrapolation of the available data with increased confidence and provides direction for additional testing.

ACKNOWLEDGMENTS

This work was supported by the United States Department of Energy through Contract No. DE-AC11-93PN38195.

APPENDIX

Strain Rate Equation For Thermally Activated Glide With Two Stage Obstacles

Environmentally assisted cracking of NiCrFe alloys X-750 and Alloy 600 has occurred in nuclear reactor components under conditions of high stress and temperatures less than about 0.35 T_m, the melting temperature. The probable mechanism for crack tip deformation under these conditions is thermally activated glide of dislocations. Details of the thermodynamics and kinetics of dislocation glide are discussed in the References.[8, 18-20]

The following development follows that of Kocks et al.[8] We consider thermally activated glide in the presence of both short and long range obstacles. Examples of long range obstacles include dislocations on parallel slip planes and large precipitate particles. Examples of short range obstacles include dislocations threading the glide plane ("forest" dislocations) and the Peierls-Nabarro stress. See Conrad[19] for a discussion of obstacles to dislocation glide.

We choose a reference state defined by a reference temperature, T_o. Above T_o the short range obstacles to dislocation glide are overcome by thermal fluctuations without the need for an applied stress greater than a threshold stress, σ_{th}, called the "athermal" stress. Below T_o thermal fluctuations are no longer sufficient acting alone to overcome short range obstacles. An additional "effective" stress, σ^*, is required.

The effective applied stress is defined by

$$\sigma^* \equiv \sigma - \sigma_{th}. \tag{A.1}$$

For temperatures below T_o the strain rate is given by

$$\dot{\varepsilon} = \dot{\varepsilon}_s \exp\left(-\frac{\Delta G(\sigma)}{kT}\right). \tag{A.2}$$

The pre-exponential factor, $\dot{\varepsilon}_s$, is a material parameter that is proportional to the density of mobile dislocations and the thermal-activation frequency. The activation enthalpy, ΔG, is given by

$$\Delta G(\sigma) = \int_{\sigma}^{\sigma_s} b\Delta a \, \delta\sigma. \tag{A.3}$$

In this equation, $b\Delta a$ is an "activation volume" where b is the Burgers vector and Δa is the activation area. In terms of the effective stress

$$\Delta G(\sigma^*) = \int_{\sigma^*}^{\sigma_s^*} b\Delta a^* \, \delta\sigma^*, \tag{A.4}$$

where

$$\begin{aligned} \sigma_s^* &= \sigma_s - \sigma_{th}, \\ \sigma^* &= \sigma - \sigma_{th}. \end{aligned} \tag{A.5}$$

Utilizing a phenomenological glide resistance profile described by Kocks et al. for short range obstacles,

$$\Delta G(\sigma^*) = F_0^* \left[1 - \left(\frac{\sigma^*}{\sigma_s^*}\right)^p\right]^q, \tag{A.6}$$

where F_o^* is the free energy necessary to overcome the short range obstacles without the aid of an external stress. In terms of the activation free enthalpy (Gibbs free energy), ΔG,

$$F_0^* \equiv \Delta G(\sigma^* = 0) = \int_0^{\sigma_s^*} b\Delta a \, \delta\sigma^*. \tag{A.7}$$

Now

$$\Delta H \equiv \Delta G + T\Delta S, \tag{A.8}$$

where ΔH is the activation enthalpy and ΔS is the activation entropy. If we assume that both ΔH and ΔS are independent of temperature, and if we choose their values at T_o, we have for all temperatures, $\Delta H = \Delta H_o^*$ and $\Delta S = \Delta S_o^*$.

Then

$$F_0^* \equiv \Delta G = \Delta H_0^* - T\Delta S_0^*. \qquad (A.9)$$

And since

$$\Delta S_0^* = \frac{\Delta H_0^*}{T_0}, \qquad (A.10)$$

$$\Delta F_0^* = \Delta H_0^*(1 - T/T_0). \qquad (A.11)$$

Then, using Eq.(A.6),

$$\frac{\Delta G}{kT} = \frac{\Delta H_0^*}{kT}\left(1 - \frac{T}{T_0}\right)\left[1 - \left(\frac{\sigma^*}{\sigma_s^*}\right)^p\right]^q, \qquad (A.12)$$

$$= \frac{\Delta H_0^*}{kT^*}\left[1 - \left(\frac{\sigma^*}{\sigma_s^*}\right)^p\right]^q,$$

where

$$\frac{1}{T^*} \equiv \frac{1}{T} - \frac{1}{T_0}. \qquad (A.13)$$

Then Eq. (A.2) becomes

$$\dot{\varepsilon} = \dot{\varepsilon}_s \exp\left\{-\frac{\Delta H_0^*}{kT^*}\left[1 - \left(\frac{\sigma^*}{\sigma_s^*}\right)^p\right]^q\right\}. \qquad (A.14)$$

In the analysis of the Shen-Shewmon and Speidel-Magdowski IGSCC crack growth data we find satisfactory data fits if we assume that q, which can have values from 1 to 2, has a value of 1.

REFERENCES

1. US Regulators Focus on Generic Threat From Inconel-600 Cracking, Nucleonics Week 30, 39(1989). p.1.
2. J.K. Sung and G.S. Was, Corrosion, 47,11(1991): pp. 824-834.
3. G.S. Was, J.K. Sung, and T.M. Angeliu, Metallurgical Transactions A, 23A, 12(1992): pp. 3343-3359.
4. T.M. Angeliu and G. S. Was, Metallurgical and Materials Transactions A, 25A, 6(1994): pp. 1169-1183.
5. J.M. Boursier, O. de Bouvier, J.M. Gras, D. Noel, R. Rios and F. Vaillant, "SCC of Alloy 600 in High Temperature Water: A Study of Mechanisms", "Corrosion-Deformation Interactions CDI 92", (Les Ulis, France, Les Editions de Physique, 1992). pp. 117-137.
6. D. Buisne et al., "Stress Corrosion Cracking in the Vessel Closure Head Penetrations of French PWR's," Sixth International Symposium on Environmental Degradation of Materials in Nuclear Power Systems - Water Reactors, R. E. Gold and E. P. Simonen, Editors, (Warrendale, PA: The Minerals, Metals and Materials Society, 1993), pp. 845-853.
7. R.A. Mulford and U.F. Kocks, Acta Metallurgica, 27, 7(1979): pp. 1125-1134.
8. U.F. Kocks, A.S. Argon and M.F. Ashby, Progress In Materials Science, 19, (New York, N.Y., Pergamon Press, 1975).
9. W. W. Gerberich and S. Shen, "Environment-Induced Cracking of Metals, Fundamental Processes: Micromechanics", Proceedings of the First International Conference on Environment-Induced Cracking of Metals, (Houston, TX: NACE, 1989), pp. 167 - 187.
10. J.W. Hutchinson, Journal of the Mechanics and Physics of Solids, 16, 1 and 5(1968): pp. 13-31, 337-347.
11. J.R. Rice and G.F. Rosengren, Journal of the Mechanics and Physics of Solids, 16, 1(1968): pp. 1-12.
12. Y. Shen and P.G. Shewmon, Corrosion, 47, 9(1991): pp. 712-718.
13. M.O. Speidel and R. Magdowski, "Stress Corrosion Cracking of Nickel Base Alloys in High Temperature Water", Sixth International Symposium on Environmental Degradation of Materials in Nuclear Power Systems - Water Reactors, R. E. Gold and E. P. Simonen, Editors, (Warrendale, PA: The Minerals, Metals and Materials Society, 1993), pp. 361-371.
14. G.L. Webb and M.M. Hall, Jr., "Pressurized Water Stress Corrosion Cracking of Alloy 600; Additional Observations on the Effects of Processing Variables," WAPD-T-3059, 1994.
15. E. Sirois and H.K. Birnbaum, Acta Metallurgica et Materialia, 40, 6(1992): pp. 1377-1385.
16. R. Bandy and D. van Rooyen, Corrosion, 40,8(1984): pp. 425-430.
17. E. Rota, F. Waelbroeck, P. Weinhold and J. Winter, Journal of Nuclear Materials, 111(1982): pp. 233-239.
18. A.H. Cotrell, Dislocations and Plastic Flow in Crystals(Oxford: Carendon Press, 1953)
19. H. Conrad, Journal of Metals, 16, 7(1964): pp. 582-588.
20. A.G. Evans and R.D. Rawlings, Physica Status Solidi, 34, 1(1969): pp. 9-31.